Meng et al. *NPG Asia Materials* (2023) 15:14
https://doi.org/10.1038/s41427-022-00441-0

NPG Asia Materials

ARTICLE Open Access

An integrated oxygen electrode derived from a flexible single-walled carbon nanotube film for rechargeable Zn-air batteries produced by electropolymerization

Yu Meng[1,2], Yi-Ming Zhao[1,2], Jin-Cheng Li[3], Chao Shi[1], Lili Zhang[1], Peng-Xiang Hou[1], Chang Liu[1] and Hui-Ming Cheng[1,4]

Abstract

The development of low-cost, high-activity, and durable integrated bifunctional flexible air electrodes for use in Zn-air batteries is both challenging and important. We report a simple and scalable electropolymerization method used to prepare an electrode material comprising heavily N-doped carbon covering single-walled carbon nanotube (N/C-SWCNT) networks. The resulting core/shell structure of the hybrid electrode enabled the flexibility, mechanics, and three-dimensional interconnected porous structure of SWCNT films while containing abundant pyridinic N, which provided excellent catalytic activity for both the oxygen reduction and evolution reactions (overpotential gap = 0.76 V). A binder-free Zn-air battery using the N/C-SWCNT film as an oxygen electrode was assembled and showed a high peak power density of 181 mW/cm^2, a high specific capacity of 810 mAh/g and stable discharge–charge cycling performance. We also constructed a flexible solid-state Zn-air battery featuring not only a high power density of 22 mW/cm^2 but also good flexibility and stability.

Introduction

With the rapid development of flexible and wearable electronics, there is an urgent need for flexible, high-density energy storage and conversion devices serving as power sources[1]. Rechargeable Zn-air batteries (ZABs) are promising candidates because of their high energy densities, low cost, and good safety[2–4]. In addition, all-solid-state flexible ZABs can be realized by using a solid electrolyte and a flexible oxygen electrode[1,5,6]. To improve the efficiencies of rechargeable ZABs, various bifunctional catalysts have been developed to accelerate the oxygen reduction/evolution reactions (ORR/OER) occurring at the oxygen electrode. Traditional oxygen electrodes for ZABs are usually prepared by dispersing a powdered catalyst and smearing it on a carbonaceous substrate such as carbon fiber paper (CFP)[7–10]. An insulating polymer binder such as Nafion is always used, which lowers the electrical conductivity and catalytic activity of the oxygen electrode[11,12]. Furthermore, the catalysts may easily fall off the substrate, especially during the gas evolution reaction, and loss of catalyst greatly degrades the cycling stability of the battery[13,14].

Recent research has been focused on the development of integrated flexible oxygen electrodes comprising free-standing carbon assemblies and tightly loaded electrocatalysts[15–17]. Carbon nanotubes (CNTs) are considered an ideal supporting matrix for an integrated oxygen electrode due to their high conductivity, good mechanical properties, and excellent chemical stability, which satisfy the requirements for electron transfer and mass transport

Correspondence: Peng-Xiang Hou (pxhou@imr.ac.cn) or Chang Liu (cliu@imr.ac.cn)
[1]Shenyang National Laboratory for Materials Science, Institute of Metal Research, Chinese Academy of Sciences, Shenyang 110016, China
[2]School of Materials Science and Engineering, University of Science and Technology of China, Hefei 230026, China
Full list of author information is available at the end of the article

even when working in a harsh environment[18,19]. Due to the inertness of the sp^2 hybridized carbon atoms they contain, CNTs show limited intrinsic catalytic activity for both the ORR and OER[20,21]. As a result, effort has been devoted to improving the activity of CNTs by heteroatom doping, defect engineering or combining them with active materials[22]. For example, Li et al. designed a porphyrin covalent organic framework covering a CNT scaffold for use as a free-standing oxygen electrode[23]. Pendashteh et al. constructed self-standing air cathodes from macroscopic CNT fibers by direct CVD spinning followed by hydrothermal modification[24]. Due to the hydrophobicity of CNTs, previously reported fabrication methods have generally involved a complex and time-consuming pretreatment process for functionalizing the inert CNT walls to graft active sites[25–27]. In addition, most CNT-based flexible oxygen electrodes are fabricated using a multiwall CNT powder or aligned multiwall CNT arrays[23,28]. These materials usually suffer from low crystallinity and low mechanical strength and have poorly interconnected networks for electron and mass transfer. Therefore, it is urgent to develop a simple and efficient method for simultaneously grafting a high density of active sites and retaining the flexibility, robustness, and stability of a CNT-based integrated oxygen electrode.

In this study, high-quality self-supporting single-walled CNT (SWCNT) films with 3D interconnected porous structures and good mechanical properties, which were prepared by floating catalyst chemical vapor deposition (FCCVD), were used as conductive scaffolds[29]. Conductive polypyrrole (PPy) was used as a precursor to grafted N-doped carbon active sites due to the high content of N[25,30]. We then developed a simple, rapid and scalable electropolymerization method with which to coat the SWCNTs with PPy, and the method can also be applied to other membrane substrates, such as CFP. After ammonization, the resulting core/shell hybrid film of N-doped carbon covering the single-wall carbon nanotubes (N/C-SWCNTs) inherits the high conductivity, flexibility, mechanical strength, and porous structure of the SWCNT film and contains a high content of exposed pyridinic N, leading to excellent catalytic activity and stability for both the ORR and OER. Large-area N/C-SWCNT films were used directly as an integrated binder-free oxygen electrode for rechargeable ZABs. The assembled aqueous ZAB had a high peak power density of 180 mW/cm^2, a high specific capacity of 810 mAh/g, and good cycling stability. In addition, a flexible solid-state ZAB was assembled by using the N/C-SWCNT film as the oxygen electrode, which demonstrated its potential for use in flexible and wearable electronics.

Results and discussion

Synthesis and characterization of the N/C-SWCNT film

Preparation of the N/C-SWCNT film is shown schematically in Fig. 1, and three steps were involved: O_2-plasma treatment, electropolymerization, and thermal pyrolysis. Self-supporting high-quality SWCNT films were prepared by an FCCVD method[31]. Figure S1 shows optical images of as-prepared SWCNT films of different sizes, demonstrating good flexibility and structural uniformity. The SWCNT film was treated with an O_2-plasma to introduce oxygen-containing functional groups, which increased its hydrophilicity and facilitated subsequent combination with the polymer (Fig. S2). The SWCNT film was then used as a working electrode and was placed in hydrochloric acid solution containing pyrrole monomer. A cycling oxidizing potential was applied to the SWCNT film, during which the pyrrole monomer in the was oxidized and electropolymerized to PPy[32]. The cyclic voltammetry (CV) curve for the electropolymerization process is shown in Fig. S3, where an increase in current at 0.66 V (versus Ag/AgCl) was observed due to polymerization of the pyrrole monomer. It took only a few minutes to form a firm coating of PPy on the surface of the SWCNT film and obtain a PPy-SWCNT film.

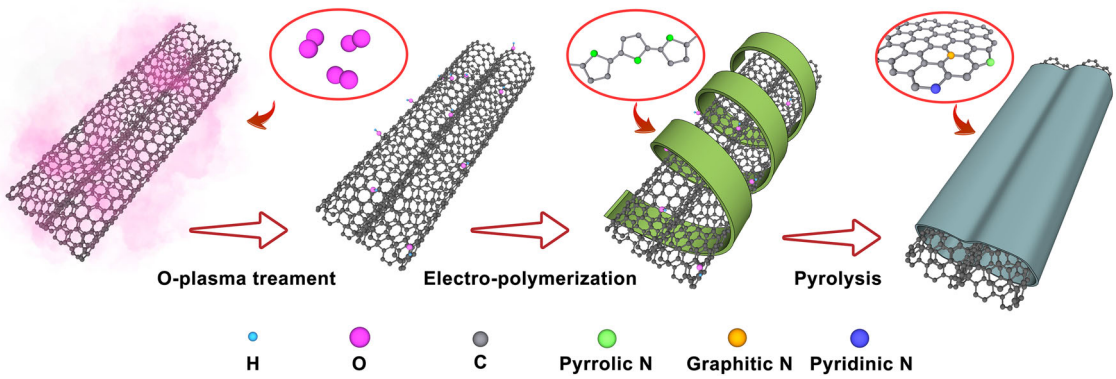

Fig. 1 Flow chart of preparation. Schematic showing preparation of the core/shell structured N/C-SWCNT film.

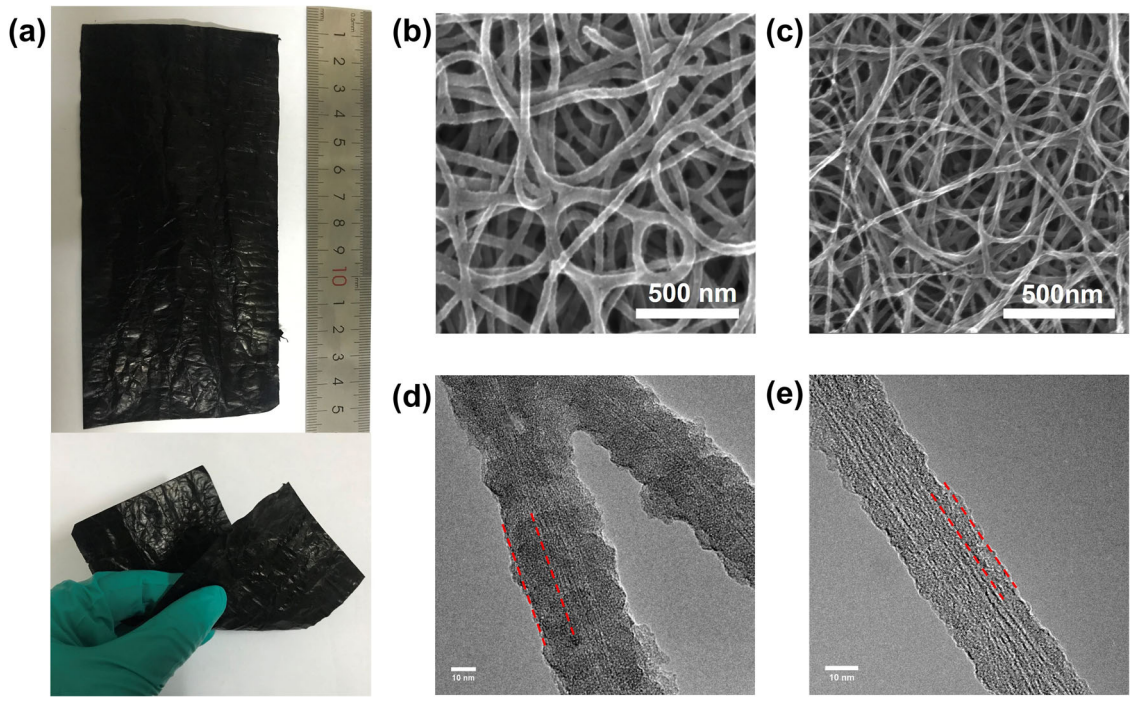

Fig. 2 Mophology characterizations. a Optical photograph of a flexible N/C-SWCNT film. **b** SEM image of PPy-SWCNTs. **c** SEM image of a N/C-SWCNT film. **d** High-resolution TEM image of PPy-SWCNTs. The PPy coating is between the dashed red lines. **e** High-resolution TEM image of N/C-SWCNT. The N-doped carbon coating is between the red lines.

The thickness of the PPy coating was easily controlled by changing the number of electropolymerization cycles (Fig. S4). Finally, the PPy-SWCNT films were heat treated under an NH_3 atmosphere to carbonize the PPy to N-doped porous carbon and obtain a N/C-SWCNT film.

Optical photographs of a large-area PPy-SWCNT film obtained after 8 electropolymerization cycles and the corresponding N/C-SWCNT film are shown in Fig. S5 and Fig. 2a. Both films inherited the macrostructure of the original SWCNT film (Fig. S1) and had good flexibility. Furthermore, the stress–strain curves in Fig. S6 show that the N/C-SWCNT film tolerated a high tensile strength of 52 MPa, which is ~11.8 times higher than that of commercial CFP (4.4 MPa). The good flexibility and high strength of the N/C-SWCNT films enable them to serve as robust air electrodes for ZABs. Scanning electron microscopy (SEM) images (Fig. 2b, c) show an interconnected network structure that is similar to that of the original SWCNT film (Fig. S7). However, the mean diameter of the filaments in PPy-SWCNT was increased to ~40 nm, much larger than the ~15 nm of the original SWCNT film (Fig. S7), which indicated that PPy was coated on the SWCNT bundles. SEM observations (Figs. S8 and S9) showed that the diameter of the filaments increased with increasing numbers of electropolymerization cycles, indicating the good controllability available with this technique. The size of a bundle of CNTs in the N/C-SWCNT film decreased to ~25 nm after pyrolysis of the PPy in an ammonia atmosphere due to partial etching by ammonia. TEM observations of the PPy-SWCNTs (Fig. 2d and Fig. S10) showed that an ~12 nm-thick PPy layer was uniformly coated on the SWCNT bundles compared with the clean surfaces of pristine SWCNTs (Fig. S11). For N/C-SWCNTs, the thickness of the coating decreased to ~6 nm (Fig. 2e), which was consistent with the SEM observations. Furthermore, the porous coating firmly covered the SWCNT bundle and formed a seamless core-shell structure. The inner SWCNT bundles retained their original structures, which is needed for quick electron transfer and good chemical stability. Additionally, the outer N-doped carbon shell contained abundant exposed active sites for the OER/ORR. The Raman spectra in Fig. S12 show a high I_G/I_D ratio of 6.85 for the N/C-SWCNT film, which is ~14 times higher than that of commercial CFP ($I_G/I_D = 0.49$) and is also superior to those for most carbonaceous supports of powdered catalysts[33–37].

The pore structure of the N/C-SWCNT film was investigated with cryogenic-nitrogen adsorption-desorption measurements. As shown in Fig. S13a, there was hysteresis in the high-pressure region ($P/P_0 = 0.8–1.0$), which was attributed to the macropores between stacked SWCNTs. There was strong absorption in the low-pressure region ($P/P_0 = 0–0.1$), which originated from the abundant micropores in N/C-SWCNTs. The N/C-SWCNT film

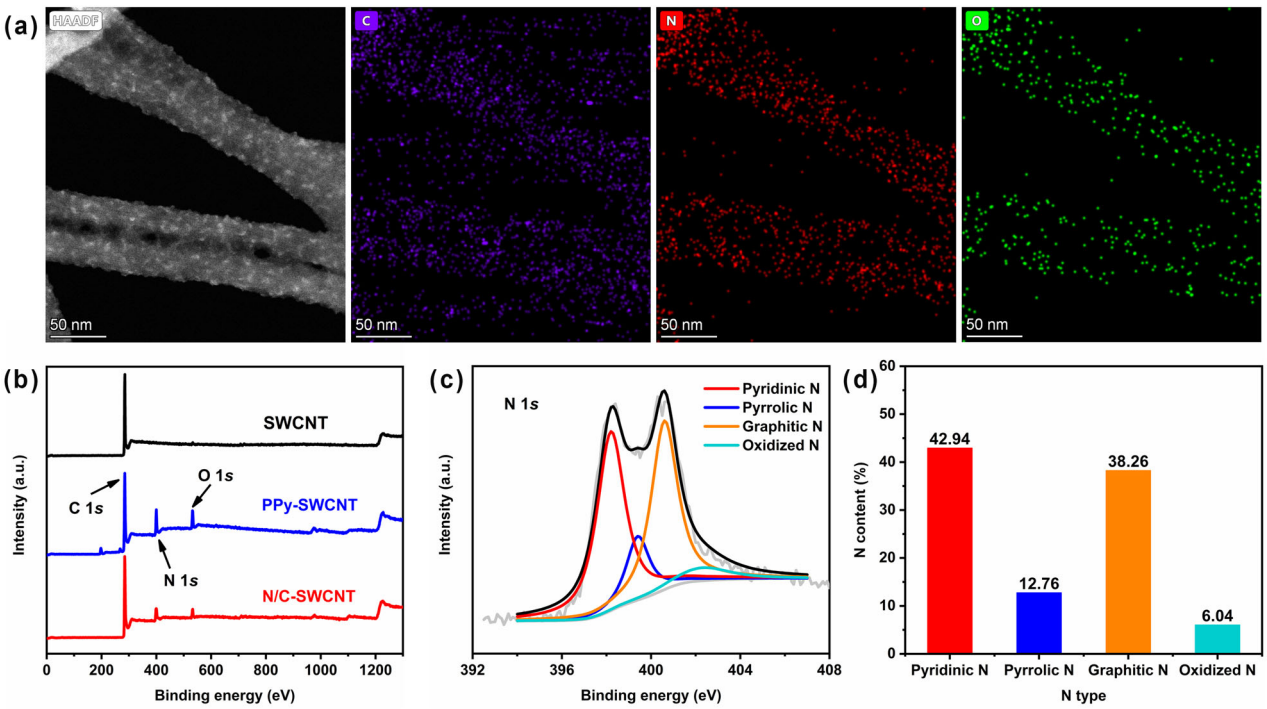

Fig. 3 Elemantal composition of N/C-SWCNT film. a STEM image and corresponding EDS elemental (C, N, and O) maps of N/C-SWCNT. **b** XPS spectra of SWCNTs, PPy-SWCNTs and N/C-SWCNTs. **c** N 1 s XPS data for N/C-SWCNT. **d** Contents of different N types in N/C-SWCNT.

showed a Brunauer–Emmett–Teller (BET) surface area of 664 m^2/g, which was much higher than that of a powdered Pt/C catalyst (158 m^2/g). Fig. S13b shows the Barrett-Joiner-Halenda (BJH) pore size distribution, and the inset shows the micropore size distribution predicted with density functional theory (DFT). The N/C-SWCNT film contained abundant micropores with diameters under 2 nm, which guaranteed mass transport in the electrode and fully exposed the N-containing active sites to the electrolyte.

To reveal the elemental composition of the N/C-SWCNT films, energy-dispersive X-ray spectroscopy (EDS) and X-ray photoelectron spectroscopy (XPS) were applied. Figure 3a shows a STEM image of a N/C-SWCNT film and the corresponding EDS elemental maps for C, N and O. Abundant elemental N was evenly distributed in the SWCNT bundle. XPS survey curves for the original SWCNT, PPy-SWCNT, and N/C-SWCNT films are shown in Fig. 3b, in which a new N 1 s peak appeared for the PPy-SWCNT and N/C-SWCNT samples. The N contents in the PPy-SWCNTs reached 14.85 at%. According to the peak positions, the N doped into the nanocarbon can be classified as pyridinic N (398.4 eV), pyrrolic N (399.1 eV), graphitic N (401.0 eV), and quaternary N^+-O^- (402.7 eV), each of which exhibited the indicated binding energy[38]. According to the N 1 s data shown in Fig. S14, N doping of PPy-SWCNT mainly provided pyrrolic N. After pyrolysis in an NH_3 atmosphere, the N content in N/C-SWCNT reached 11.34 at% (Fig. S15), which is a high level for carbon-based N-doped catalysts. At the same time, the N/C-SWCNT film gave a N 1 s spectrum (Fig. 3c) that was obviously different from that of PPy-SWCNT. The contents of the different types of doped N were calculated from their integrated peak areas, and the results are shown in Fig. 3d. Pyridinic N (42.94%) and graphitic N (38.26%) were dominant, and they are believed to be highly active sites for ORR catalysis[39,40].

ORR and OER performance of the N/C-SWCNT film

The electrocatalytic ORR activity of the N/C-SWCNT film was evaluated by rotating disk electrode (RDE) and rotating ring-disk electrode (RRDE) techniques, and a commercial Pt/C catalyst was used as the benchmark. The process used for preparation of the working electrodes is described in Supplementary Note 1. We investigated the thickness of the porous N-doped carbon (electropolymerization cycles) and the pyrolysis temperature and determined their effects on the ORR performance of the N/C-SWCNT film. As shown in Figs. S16, S17 and S18, the N/C-SWCNT film prepared with 8 electropolymerization cycles and pyrolysis at 700 °C showed the best ORR performance. Even though the N/C-SWCNT film subjected to 16 cycles contained the highest N

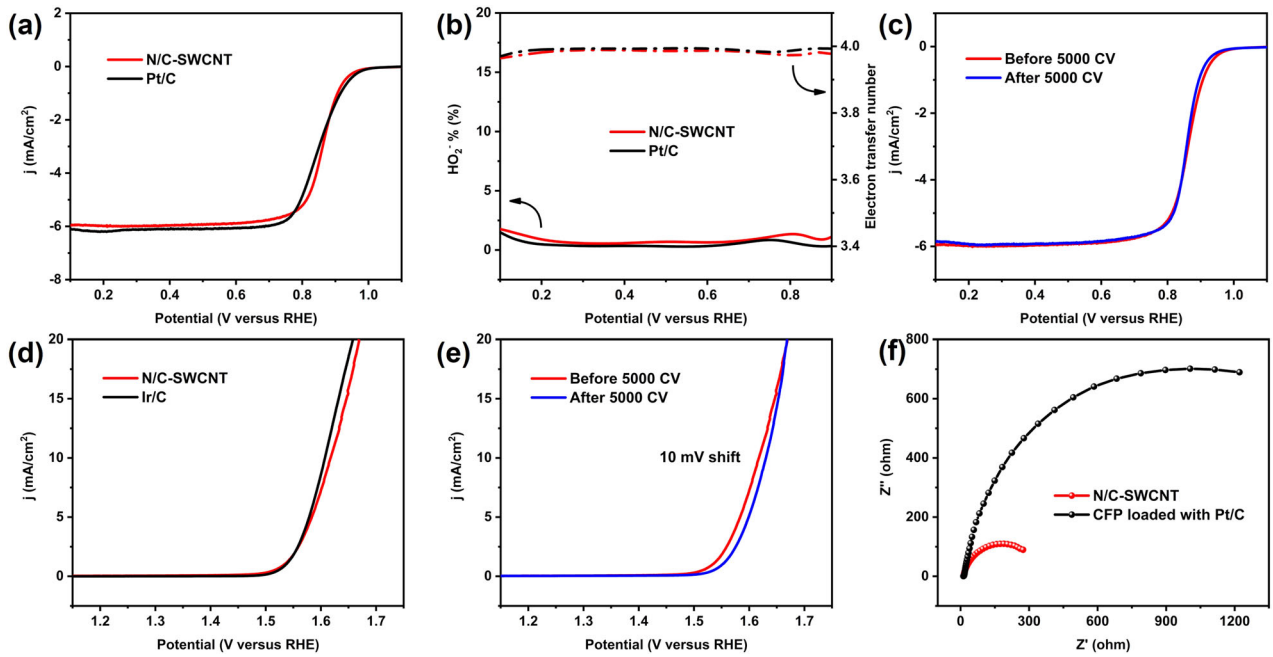

Fig. 4 Catalytic performances and conductivity of N/C-SWCNT film. a ORR polarization curves and **b** peroxide yields and electron transfer numbers for N/C-SWCNT and Pt/C. **c** Initial ORR polarization curve for N/C-SWCNT and that after 5000 CV cycles. **d** OER polarization curves for N/C-SWCNT and Ir/C. **e** Initial OER polarization curve for N/C-SWCNT and that after 5000 CV cycles. **f** Nyquist profiles for a N/C-SWCNT film and CFP loaded with a Pt/C catalyst.

content (Fig. S15), its onset potential was the lowest among the four samples. This is because the overly thick and aggregated PPy layer (Fig. S9) disfavored ORR catalysis.

We also studied the ORR and OER performance of the N/C-SWCNT film prepared with 8 electropolymerization cycles. Figure 4a shows the linear scan voltammogram (LSV) polarization curves recorded with a disk electrode. The N/C-SWCNT film showed a positive half-wave potential ($E_{1/2}$) of 0.86 V, which was comparable to that of Pt/C (0.85 V). However, the pristine SWCNT film and intermediate PPy-SWCNT film had half-wave potentials of 0.57 V and 0.70 V, respectively (Fig. S19), which were much lower than that of the N/C-SWCNT film and indicated the importance of transforming pyrrolic N to pyridinic N by pyrolysis. The Tafel plot for N/C-SWCNT derived from the polarization curve (Fig. S20) showed a Tafel slope of 68 mV/dec, which was even better than that of Pt/C (72 mV/dec). Figure 4b shows the HO_2^- yield and calculated electron transfer number for the N/C-SWCNT film and for Pt/C. The N/C-SWCNT film showed a very low HO_2^- yield below 3%, which was similar to that of Pt/C. The number of electrons transferred calculated from the HO_2^- yield of the N/C-SWCNT film was nearly 4.0, which was consistent with the result calculated with the Koutecky–Levich (K–L) equation based on the RDE curves (Fig. S21) for different rotation rates, indicating efficient kinetics toward the ORR. We further evaluated the stability of the N/C-SWCNTs. Figure 4c shows the initial ORR polarization curve and that seen after 5000 CV cycles. The $E_{1/2}$ of N/C-SWCNT remained almost constant and was even more stable than that for the Pt/C catalyst (27 mV decay) (Fig. S22a), demonstrating excellent ORR stability.

In addition to the ORR catalytic activity, the N/C-SWCNT film also showed good OER catalytic activity. The potential seen for an oxidation current density of 10 mA/cm^2 during OER ($E_{j=10}$) is usually used as a benchmark with which to evaluate the OER performance. As shown in Fig. 4d, the $E_{j=10}$ of N/C-SWCNTs was 1.62 V and only 10 mV higher than that of an Ir/C catalyst (1.61 V). The Tafel plots in Fig. S23 show that the Tafel slope of N/C-SWCNT was 67 mV/dec, which was comparable to that of Ir/C (51 mV/dec). We also evaluated the stability of the N/C-SWCNT film for OER by performing 5000 CV cycles, and the polarization curves are shown in Fig. 4e. There was only a 10 mV decay of $E_{j=10}$ for the N/C-SWCNTs, while Ir/C showed a 25 mV decay (Fig. S22b). This demonstrated that the N/C-SWCNTs have excellent OER stability. The total overpotential ($\Delta E = E_{j=10} - E_{1/2}$) of the N/C-SWCNT film, which represents the overall catalytic performance for a bifunctional oxygen catalyst, reached 0.76 V, the same as that of precious metal Pt/C-Ir/C catalysts ($\Delta E = 0.76$ V), and ranked highest among the previously reported metal-free catalysts listed in Supplementary Table 1. Because of this

excellent bifunctional catalytic activity and the free-standing integrated morphology, the N/C-SWCNT film can be used directly as an oxygen electrode. The N/C-SWCNT film also had an even lower impedance than a Pt/C catalyst loaded on CFP, which indicated better conductivity (Fig. 4f). We applied the electropolymerization method to CFP (eight cycles, 700 °C pyrolysis) to verify its universality for other membrane substrates. As shown in Fig. S24 and Fig. S25, N-doped carbon covering the CFP was obtained, indicating that the electropolymerization method is also applicable for other membrane substrates.

Performance of Zn-air batteries assembled with N/C-SWCNT films

We further fabricated a rechargeable ZAB by using the N/C-SWCNT film as a catalytic layer (denoted N/C-SWCNT ZAB). For comparison, a Pt/C-Ir/C catalyst-based ZAB was also fabricated (denoted Pt/C-Ir/C ZAB). The detailed fabrication process is described in Supplementary Note 2. Figure 5a shows the open circuit voltages (OCVs) of the rechargeable ZABs. We can see that the N/C-SWCNT ZAB had a higher OCV (1.43 V) than the Pt/C-Ir/C ZAB (1.37 V). Figure 5b shows the polarization curves and the power densities derived for these two ZABs. The peak power density of the N/C-SWCNT ZAB was 181 mW/cm^2, which was higher than that of the Pt/C-Ir/C ZAB (142 mW/cm^2). The specific capacities (SCs) of the ZABs were calculated according to their galvanostatic discharge curves at 10 mA/cm^2 (Fig. 5c) by normalizing to the mass consumption of Zn. The N/C-SWCNT ZAB had a specific capacity of 810 mAh/g, higher than that of the Pt/C-Ir/C ZAB (731 mAh/g); this demonstrated the superiority of an N/C-SWCNT film as an integrated ZAB electrode. Good cycling stability is of great significance for practical applications of rechargeable ZABs. We therefore tested ZABs with long-term galvanostatic discharge–charge cycling at 10 mA/cm^2 to evaluate their stabilities. As shown in Fig. 5d, the N/C-SWCNT ZAB retained a stable discharge/charge voltage gap of 0.77 V (discharge: 1.16 V; charge: 1.93 V) after 100 h of discharge–charge cycling, which was smaller than that of Pt/C-Ir/C ZAB (0.89 V after 65 h) (Fig. S26). In Supplementary Table 2, we summarize the performance of representative ZABs assembled by using metal-free bifunctional oxygen electrocatalysts. Our N/C-SWCNT ZAB performed among the best catalysts on the list in terms of peak power, specific capacity, stability, and discharge–charge voltage gap, demonstrating that the N/C-SWCNT film is an excellent integrated bifunctional oxygen electrocatalyst.

Due to its robustness and excellent flexibility inherited from the high-quality SWCNT film, the N/C-SWCNT film was directly used as a catalytic layer with which to assemble a flexible solid-state Zn-air battery by simply

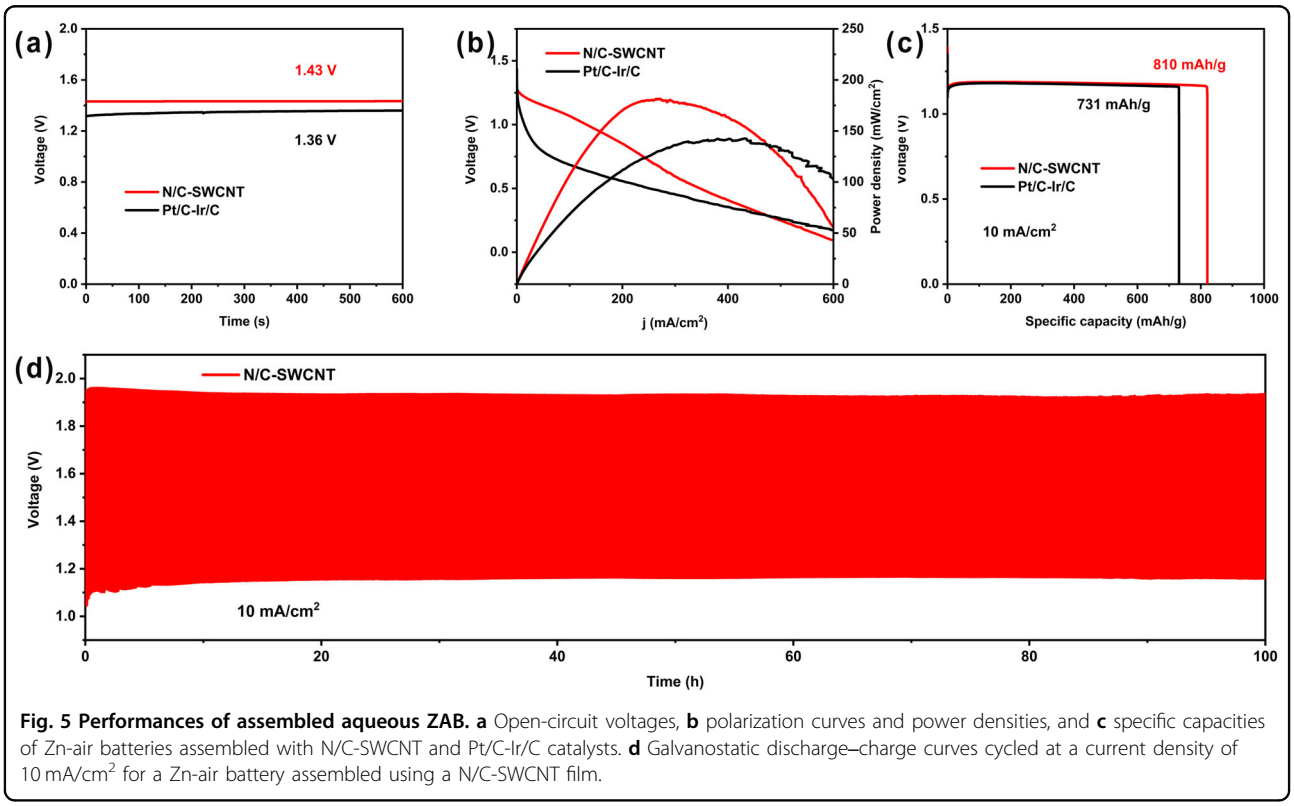

Fig. 5 Performances of assembled aqueous ZAB. a Open-circuit voltages, **b** polarization curves and power densities, and **c** specific capacities of Zn-air batteries assembled with N/C-SWCNT and Pt/C-Ir/C catalysts. **d** Galvanostatic discharge–charge curves cycled at a current density of 10 mA/cm^2 for a Zn-air battery assembled using a N/C-SWCNT film.

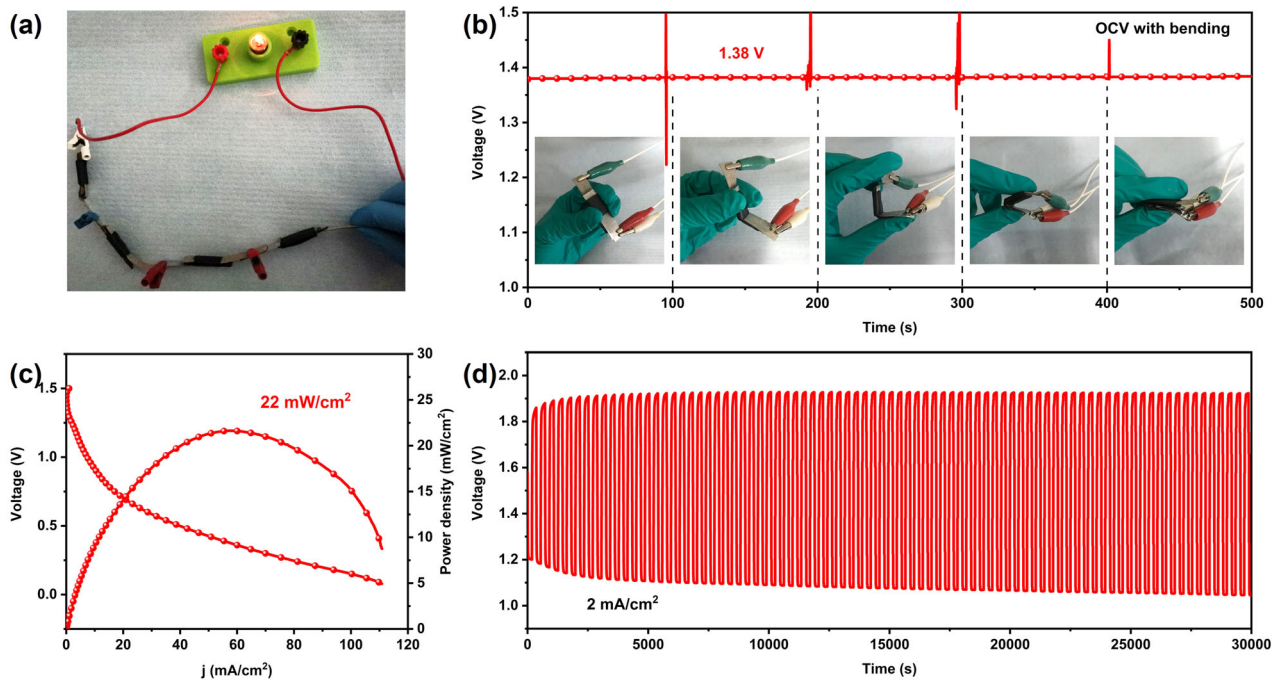

Fig. 6 Performances of assembled solid-state ZAB. a Optical photograph of a small bulb lit with a series of flexible solid-state N/C-SWCNT ZABs. **b** OCV of the solid-state Zn-air battery with different bending states. **c** Polarization curves and power density of the solid-state N/C-SWCNT ZAB. **d** Galvanostatic discharge–charge cycling curves obtained with a current density of 2 mA/cm^2 for the solid-state N/C-SWCNT ZAB.

integrating a Zn plate, a gel electrolyte, N/C-SWCNTs and a nickel foam current collector without using any additional binders. The detailed fabrication process is described in Supplementary Note 2. As shown in Fig. 6a, a bulb was lit by a series of flexible solid-state Zn-air batteries. When the battery was bent to various angles, a stable OCV of 1.38 V was retained (Fig. 6b). The assembled battery also had a high peak power density of 22 mW/cm^2 (Fig. 6c). To evaluate the stabilities of the Zn-air batteries, cyclic galvanostatic discharge–charge tests were conducted at 2 mA/cm^2 (360 s/cycle). As shown in Fig. 6d, the solid-state Zn-air battery showed a stable cycling curve. The charge voltage stabilized at 1.9 V, and the discharge voltage was ~1.1 V with a slight decay, which was probably caused by dehydration of the gel electrolyte. These results indicated that our N/C-SWCNT film shows promise for use as an integrated electrode in flexible and wearable electronic devices.

Conclusions

We have developed an electropolymerization strategy with which to fabricate a large-scale core/shell-structured N/C-SWCNT film for use as bifunctional oxygen electrodes in rechargeable Zn-air batteries. The obtained N/C-SWCNT films showed three-dimensional interconnected pore structures, good flexibilities, high strengths, and ultrahigh active N contents of 11.34 at%. As a result, they showed good ORR and OER catalytic activities with a small overpotential gap of 0.76 V and excellent stability. When directly used as a catalytic layer in a rechargeable ZAB, the assembled ZAB had a high power density, high specific capacity and excellent long-term discharge–charge stability. A solid-state Zn-air battery with good flexibility and performance stability was fabricated by using the N/C-SWCNT film as an integrated electrode. This work provides an easy and scalable way to synthesize a high-efficiency bifunctional oxygen electrocatalyst.

Experimental

Preparation of high-quality SWCNT films

Free-standing SWCNT films were prepared by the floating catalyst chemical vapor deposition method. Ferrocene and thiophene were dissolved in toluene in a weight ratio of 2.5:0.7:91 and served as the catalyst precursor, growth promoter, and carbon source, respectively. The growth temperature was 1100 °C. During SWCNT growth, the solution was injected into the reactor at a rate of 0.74 ml/h. Simultaneously, 7000 standard cubic centimeters per minute (sccm) hydrogen and 8.25 sccm ethylene (the second carbon source) were introduced. The SWCNT films were collected on a steel mesh installed downstream from the reactor. Large-area SWCNT films were collected on a filter membrane by a continuous collection process.

Preparation of N/C-SWCNT films

The SWCNT film was first treated with O_2-plasma for 200 s. The SWCNT film was then used as a working electrode, and a titanium plate and an Ag/AgCl electrode served as the counter electrode and reference electrode, respectively. The three-electrode system was placed in a glass container containing 0.1 M hydrochloric acid solution and 0.1 M pyrrole monomer. A cycling oxidizing potential (potential window: 0~1.2 V versus Ag/AgCl, sweep speed: 50 mV/s) was applied to the SWCNT film during the electropolymerization process. During electropolymerization, the pyrrole monomer polymerized and coated the SWCNTs. The film that underwent electropolymerization was then washed with deionized water, dried at 60 °C for 10 h and denoted PPy-SWCNT. Finally, the PPy-SWCNT films were heat treated at 700 °C under an NH_3 atmosphere for 1 h to obtain the N/C-SWCNT film.

Acknowledgements
This work was supported by the National Natural Science Foundation of China (Grants 51872293, 52072375, 52130209), Liaoning Revitalization Talents Program (XLYC2002037), and Basic Research Project of Natural Science Foundation of Shandong Province, China (ZR2019ZD49).

Author details
[1]Shenyang National Laboratory for Materials Science, Institute of Metal Research, Chinese Academy of Sciences, Shenyang 110016, China. [2]School of Materials Science and Engineering, University of Science and Technology of China, Hefei 230026, China. [3]Faculty of Chemical Engineering, Yunnan Provincial Key Laboratory of Energy Saving in Phosphorus Chemical Engineering and New Phosphorus Materials, Kunming University of Science and Technology, Kunming 650500, China. [4]Faculty of Materials Science and Energy Engineering/Institute of Technology for Carbon Neutrality, Shenzhen Institute of Advanced Technology, Chinese Academy of Sciences, Shenzhen 518055, China

Author contributions
Y.M. wrote the manuscript, evaluated the catalytic activities with electrochemical measurements, and examined the mechanism for catalytic activity. Y.-M.Z. and L.Z. conducted structural analyses of the catalysts using TEM, STEM, and EDS. Y.M. and J.-C.L. conceived the idea for this study. C.S. grew a large-area SWCNT film and characterized the catalytic film using XPS and Raman spectroscopy. P.-X.H., C.L., and H.-M.C. designed the methodology used to reach the conclusions. All other authors contributed to data collection and interpretation and critically reviewed the manuscript. All authors approved the final version of the manuscript and agree to be accountable for all aspects of the work and ensure that questions related to the accuracy or integrity of any part of the work are appropriately investigated and resolved.

Conflict of interest
The authors declare no competing interests.

Publisher's note
Springer Nature remains neutral with regard to jurisdictional claims in published maps and institutional affiliations.

Supplementary information The online version contains supplementary material available at https://doi.org/10.1038/s41427-022-00441-0.

Received: 29 July 2022 Revised: 7 October 2022 Accepted: 14 October 2022.
Published online: 31 March 2023

References
1. Pan, J. et al. Advanced architectures and relatives of air electrodes in Zn–Air batteries. *Adv. Sci.* **5**, 1700691 (2018).
2. Li, H. F. et al. Advanced rechargeable zinc-based batteries: recent progress and future perspectives. *Nano Energy* **62**, 550–587 (2019).
3. Fu, J. et al. Electrically rechargeable Zinc-air batteries: progress, challenges, and perspectives. *Adv. Mater.* https://doi.org/10.1002/adma.201604685 (2017).
4. Huang, Q. K. et al. Co3O4/Mn(3)O(4)hybrid catalysts with heterointerfaces as bifunctional catalysts for Zn-air batteries. *J. Energy Chem.* **68**, 679–687 (2022).
5. Wang, Y. J., Cao, Q. H., Guan, C. & Cheng, C. W. Recent advances on self-supported arrayed bifunctional oxygen electrocatalysts for flexible solid-state Zn-Air batteries. *Small* https://doi.org/10.1002/smll.202002902 (2020).
6. Zhao, S. et al. All-in-one and bipolar-membrane-free acid-alkaline hydrogel electrolytes for flexible high-voltage Zn-air batteries. *Chem. Eng. J.* **430**, 132718 (2022).
7. Tian, X. L., Lu, X. F., Xia, B. Y. & Lou, X. W. Advanced electrocatalysts for the oxygen reduction reaction in energy conversion technologies. *Joule* **4**, 45–68 (2020).
8. Li, B. et al. String of pyrolyzed ZIF-67 particles on carbon fibers for high-performance electrocatalysis. *Energy Storage Mater.* **25**, 137–144 (2020).
9. Guan, C. et al. Hollow Co 3 O 4 nanosphere embedded in carbon arrays for stable and flexible solid-state Zinc-air batteries. *Adv. Mater.* **29**, 1704117 (2017).
10. Guan, C. et al. Decorating Co/CoNx nanoparticles in nitrogen-doped carbon nanoarrays for flexible and rechargeable zinc-air batteries. *Energy Storage Mater.* **16**, 243–250 (2019).
11. Shinde, S. S. et al. Unveiling dual-linkage 3D hexaiminobenzene metal-organic frameworks towards long-lasting advanced reversible Zn-air batteries. *Energy Environ. Sci.* **12**, 727–738 (2019).
12. Yan, X. X., Ha, Y. & Wu, R. B. Binder-free air electrodes for rechargeable Zinc-air batteries: recent progress and future perspectives. *Small Methods* https://doi.org/10.1002/smtd.202000827 (2021).
13. Ma, T. Y., Dai, S. & Qiao, S. Z. Self-supported electrocatalysts for advanced energy conversion processes. *Mater. Today* **19**, 265–273 (2016).
14. He, Y. et al. In-situ observation of the gas evolution process on the air electrode of Zn-air batteries during charging. *Chem. Eng. J.* **427**, 130862 (2022).
15. Liu, Q., Wang, Y., Dai, L. & Yao, J. Scalable fabrication of nanoporous carbon fiber films as bifunctional catalytic electrodes for flexible Zn-Air batteries. *Adv. Mater.* **28**, 3000–3006 (2016).
16. Zeng, S. et al. All-in-one bifunctional oxygen electrode films for flexible Zn-air batteries. *Small* https://doi.org/10.1002/smll.201803409 (2018).
17. Li, J.-C. et al. A 3D bi-functional porous N-doped carbon microtube sponge electrocatalyst for oxygen reduction and oxygen evolution reactions. *Energy Environ. Sci.* **9**, 3079–3084 (2016).
18. Kumar, S. et al. Carbon nanotubes: a potential material for energy conversion and storage. *Prog. Energy Combust. Sci.* **64**, 219–253 (2018).
19. Yan, L. et al. Integrating trifunctional Co@NC-CNTs@NiFe-LDH electrocatalysts with arrays of porous triangle carbon plates for high-power-density rechargeable Zn-air batteries and self-powered water splitting. *Chem. Eng. J.* **446**, 137049 (2022).
20. Wang, L. & Pumera, M. Residual metallic impurities within carbon nanotubes play a dominant role in supposedly 'metal-free' oxygen reduction reactions. *Chem. Commun.* **50**, 12662–12664 (2014).
21. Cheng, Y., Zhang, J. & Jiang, S. P. Are metal-free pristine carbon nanotubes electrocatalytically active? *Chem. Commun.* **51**, 13764–13767 (2015).
22. Arafat, Y., Azhar, M. R., Zhong, Y. J., Tade, M. O. & Shao, Z. P. Metal-free carbon based air electrodes for Zn-air batteries: recent advances and perspective. *Mater. Res. Bull.* https://doi.org/10.1016/j.materresbull.2021.111315 (2021).
23. Li, B. Q. et al. A porphyrin covalent organic framework cathode for flexible Zn-air batteries. *Energy Environ. Sci.* **11**, 1723–1729 (2018).
24. Pendashteh, A., Palma, J., Anderson, M., Vilatela, J. J. & Marcilla, R. Doping of self-standing CNT fibers: promising flexible air-cathodes for high-energy-density structural Zn–Air batteries. *ACS Appl. Energy Mater.* **1**, 2434–2439 (2018).
25. Li, J.-C. et al. N-doped carbon nanotubes containing a high concentration of single iron atoms for efficient oxygen reduction. *NPG Asia Mater.* **10**, e461–e461 (2018).
26. Zeng, S. et al. Crosslinked carbon nanotube aerogel films decorated with cobalt oxides for flexible rechargeable Zn–Air batteries. *Small* **13**, 1700518 (2017).

27. Jin, Q., Ren, B., Cui, H. & Wang, C. Nitrogen and cobalt co-doped carbon nanotube films as binder-free trifunctional electrode for flexible zinc-air battery and self-powered overall water splitting. *Appl. Catal. B* **283**, 119643 (2021).
28. Yan, Y. et al. Bifunctional nickel ferrite-decorated carbon nanotube arrays as free-standing air electrode for rechargeable Zn–air batteries. *J. Mater. Chem. A* **8**, 5070–5077 (2020).
29. Cheng, H. M. et al. Large-scale and low-cost synthesis of single-walled carbon nanotubes by the catalytic pyrolysis of hydrocarbons. *Appl. Phys. Lett.* **72**, 3282–3284 (1998).
30. Wu, G., More, K. L., Johnston, C. M. & Zelenay, P. High-performance electrocatalysts for oxygen reduction derived from polyaniline, iron, and cobalt. *Science* **332**, 443–447 (2011).
31. Meng, Y. et al. Fluorination-assisted preparation of self-supporting single-atom Fe-N-doped single-wall carbon nanotube film as bifunctional oxygen electrode for rechargeable Zn-Air batteries. *Appl. Catal. B* **294**, 120239 (2021).
32. Noftle, R. E. & Pletcher, D. The mechanism of electrodeposition of composite polymers including polypyrrole. *J. Electroanal. Chem. Interfacial Electrochem.* **227**, 229–235 (1987).
33. Li, Q. et al. Biomass waste-derived 3D metal-free porous carbon as a bifunctional electrocatalyst for rechargeable Zinc-air batteries. *ACS Sustain. Chem. Eng.* **7**, 17039–17046 (2019).
34. Gao, Y., et al. N,P co-doped hollow carbon nanofiber membranes with superior mass transfer property for trifunctional metal-free electrocatalysis. *Nano Energy* https://doi.org/10.1016/j.nanoen.2019.103879 (2019).
35. Wang, H. F., Tang, C. & Zhang, Q. Template growth of nitrogen-doped mesoporous graphene on metal oxides and its use as a metal-free bifunctional electrocatalyst for oxygen reduction and evolution reactions. *Catal. Today* **301**, 25–31 (2018).
36. Qian, Y. et al. A metal-free ORR/OER bifunctional electrocatalyst derived from metal-organic frameworks for rechargeable Zn-Air batteries. *Carbon* **111**, 641–650 (2017).
37. Zhou, Z., Chen, A., Fan, X., Kong, A. & Shan, Y. Hierarchical porous N-P-coupled carbons as metal-free bifunctional electro-catalysts for oxygen conversion. *Appl. Surf. Sci.* **464**, 380–387 (2019).
38. Li, J.-C. et al. Highly dispersive cerium atoms on carbon nanowires as oxygen reduction reaction electrocatalysts for Zn–air batteries. *Nano Lett.* **21**, 4508–4515 (2021).
39. Guo, D. H. et al. Active sites of nitrogen-doped carbon materials for oxygen reduction reaction clarified using model catalysts. *Science* **351**, 361–365 (2016).
40. Li, M., Liu, Z., Wang, F. & Xuan, J. The influence of the type of N dopping on the performance of bifunctional N-doped ordered mesoporous carbon electrocatalysts in oxygen reduction and evolution reaction. *J. Energy Chem.* **26**, 422–427 (2017).